10-1-2003

FEM Modeling of Induction Hardening Processes in Steel

J. Yuan

J. Kang

Yiming Rong
Worcester Polytechnic Institute, rong@wpi.edu

Richard D. Sisson Jr.
Worcester Polytechnic Institute, sisson@wpi.edu

FEM Modeling of Induction Hardening Processes in Steel

J. Yuan, J. Kang, Y. Rong, and R.D. Sisson, Jr.

(Submitted 25 March 2003)

A modeling system for analyzing the integrated induction hardening processes was developed based on a general-purpose finite element program, with the capability to analyze the whole process from electromagnetic-induced thermal heating to final hardening. A coupled electromagnetic-thermal model was applied to study the induction heating process, which includes consideration of nonlinear material characteristics on temperature. Also, arrangement of AC current density distribution was conducted to simulate practical induction coil structure and magnetic concentrator effects to achieve desired heating patterns for later quenching and hardening analysis. Quenching analysis can provide cooling curve at any location in a heat-treated workpiece based on heat transfer principles. In hardening analysis, phase transformation was studied and an algorithm was developed to determine volumetric content of micro-structural constituents formed from austenitized phase in quenching process, based on analysis of the interaction between cooling curve and material time-temperature-transformation (TTT) diagram. Finally, hardness value was converted from martensite content based on a developed formulation. Validation was preliminary conducted based on comparison of hardening pattern of induction hardening of an automotive spindle with complex surface.

Keywords electromagnetic-thermal analysis, FEM modeling, induction hardening, phase transformation, quenching analysis

1. Introduction

Modeling of induction hardening is a complex problem, which involves numerically solving Maxwell's equations for electromagnetic field coupled with heat transfer for modeling the product thermal process. The system is inevitably highly nonlinear due to the temperature-dependent material properties of the workpiece. In the past, more attention was paid to numerical simulation than to modeling of specific aspects of the induction-hardening problem; little effort has been given to modeling the integrated process from heating to final hardening. Numerical simulation of the magnetic field was ever conducted[1] to provide valuable analysis for the magnetic vector potential which is an important parameter for eddy current and Joule heat determination. Simulation of induction heating has been carried out[2] and provided models for solving coupled electromagnetic/thermal analysis. Also, quenching and phase transformation process has been simulated[3] and the Koistinen-Marburger law[4] and Avrami[5] equation were applied for determining volume fraction of micro-constituents formed in the cooling process. However, few studies were found to predict the hardness distribution using numerical simulation.

In the present effort, an integrated finite element analysis (FEA) based modeling system has been developed with the capability to simulate the electromagnetic field induced heating process, austenite state holding processes, and severe quenching processes. Also the volume fraction of micro-constituents such as martensite formed in the quench cooling process, and final hardness distribution (pattern) in the workpiece can be determined by using the model. Through proper arrangement of input AC current density distribution, the desired hardening patterns for special complex surface can be obtained. The goal of the modeling system is to guide the design of real induction systems.

J. Yuan, J. Kang, Y. Rong, and **R.D. Sisson, Jr**., Department of Mechanical Engineering, Worcester Polytechnic Institute, Worcester, MA 01609. Contact e-mail: ynjky@wpi.edu.

2. Mathematical Model

Modeling of induction hardening system consists of several steps (Fig. 1). Electromagnetic analysis includes the electromagnetic field induced from input AC power to coil, eddy current induced in the workpiece from electromagnetic field, and Joule heat generated from eddy current. Thermal analysis includes a heating process coupled with electromagnetic analysis, austenization holding analysis used for reduction temperature difference on the workpiece surface, and quenching process for phase transformation. Hardness analysis consists of the calculation of the volume fraction of martensite, pearlite, and bainite formed in quenching process and hardness value determination based on martensite content. The computational formulation for each of these processes is described in this section.

2.1 Electromagnetic Analysis

Complex electromagnetic equations can be greatly simplified based on magnetic vector potential A.[6] All the quantities related to the inducting Joule heat can be traced, based on the AC current, I, input to the induction coil. A can be expressed with Biot-Savart law:

$$A = \frac{\mu_0 \cdot I}{4\pi} \int_s \frac{dl}{|r|} \quad \text{(Eq 1)}$$

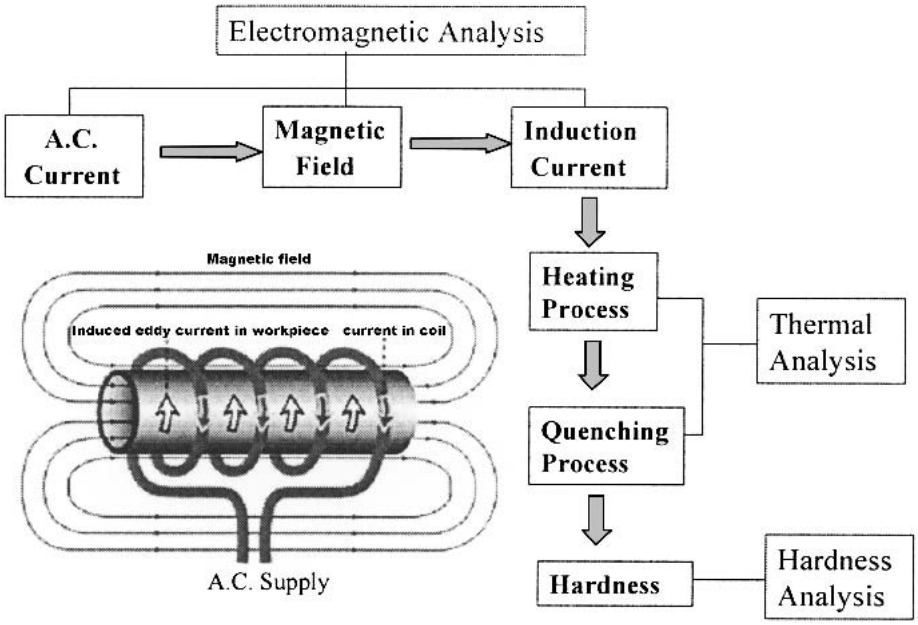

Fig. 1 Modeling process for induction hardening

Based on Gauss' law, the magnetic flux density B is:

$$B = \nabla \times A \quad \text{(Eq 2)}$$

From Faraday's law, the electricity intensity E and magnetic field density H are:

$$\nabla \times E = -\frac{\partial B}{\partial t} \quad \text{(Eq 3)}$$

$$H = B/\mu \quad \text{(Eq 4)}$$

Based on Ampere's circuit law, the current density, J, induced in the workpiece is:

$$J = \nabla \times H - \frac{\partial(\varepsilon \cdot E)}{\partial t} \quad \text{(Eq 5)}$$

After a mathematical manipulation of the above formulas, the relationship between the magnetic vector potential, A, and the induced current density, J, becomes:

$$J = \nabla \times \left(\frac{1}{\mu}\nabla \times A\right) + \sigma\frac{\partial A}{\partial t} \quad \text{(Eq 6)}$$

Finally, Joule heat generated from eddy current is:

$$Q_{\text{induction}} = \frac{J^2}{\sigma} \quad \text{(Eq 7)}$$

where μ, ε, and σ are the magnetic permeability, permittivity, and electrical conductivity of the medium, respectively. These properties are all temperature dependent, and this classifies the electromagnetic analysis as a highly nonlinear problem. With the Joule heat as the heating source, thermal analysis can be conducted next.

2.2 Thermal Analysis

Thermal analysis includes modeling the processes of heating, holding, and water quenching. The heating process is coupled with the electromagnetic conversion processes. In the heating process, the heat conduction effect is the main issue to be considered because the heating cycle is generally as short as several seconds. The conduction equation is:

$$\rho \cdot c_p \cdot \frac{\partial T}{\partial t} = k \cdot \nabla^2 T + Q_{\text{induction}} \quad \text{(Eq 8)}$$

where $Q_{\text{induction}}$ is the Joule heat from the electromagnetic process; ρ, c_p, and k are the material density, specific heat, and thermal conductivity, respectively.

The induction heating time is so short that overheating is often found concave of the workpiece with complex geometry due to the heat concentration effect at these locations. The holding process is necessary to decrease the temperature difference between the workpiece surface and inside layers through heat transfer effects (conduction, free air convection, and radiation). During the holding process, the AC power is shut off and the austenitized workpiece is held in air for about 1 s before quenching. For inside locations of the workpiece, only heat conduction effect needs to be considered and governing equation is:

$$\rho \cdot c_p \cdot \frac{\partial T}{\partial t} = k \cdot \nabla^2 T \quad \text{(Eq 9)}$$

On workpiece surfaces, the heat conduction, radiation, and free convection effects are all needed. The governing equation is:

$$\rho \cdot c_p \cdot \frac{\partial T}{\partial t} = k \cdot \nabla^2 T - S \cdot \delta \cdot \xi \cdot F \cdot (T^4 - T_{air}^4) - S \cdot h \cdot (T - T_{air}) \quad \text{(Eq 10)}$$

where S is the surface on which heat transfer is conducted; δ, ξ, and h are the thermal emissivity of the surface, Stefan-Boltzmann constant, and freely convective exchange coefficient, respectively.

The freely convective exchange coefficient is highly dependent on the temperature difference between the workpiece and air. It can be determined from:

$$h = \frac{k}{L} \cdot Nu \quad \text{(Eq 11)}$$

where k is thermal conductivity of the medium, L is the characteristic length of the workpiece, and Nu is the Nusselt number that can be determined from:

$$Nu = \left\{ 0.6 + \frac{0.387 Ra^{1/6}}{[1 + (0.559/Pr)^{9/16}]^{8/27}} \right\}^2 \quad \text{(Eq 12)}$$

$$Pr = \frac{\mu c_p}{k} \quad \text{(Eq 13)}$$

$$Ra = \frac{g\beta}{\alpha \nu} L^3 (T_{wp} - T_{air}) \quad \text{(Eq 14)}$$

where Pr is Prandtl number, Ra is Rayleigh number, μ, ν, α, β, and g are the air viscosity, air kinetic viscosity, air thermal diffusivity, air thermal expansion coefficient, and gravitational acceleration, respectively.

For the quenching process, the basic governing equations are still Eq 9 or Eq 10, except quench media is not air, but other liquids such as water or oil. The goal of modeling the quenching process is to analyze the cooling curves of the workpiece for late hardness.

2.3 Hardening Analysis

Hardness prediction is a complex process that involves analysis of interaction of cooling-curves (CC) with temperature-time-transformation (TTT) diagrams (Fig. 2). The CC curves at any location in the workpiece can be determined from numerical simulation or experimental test if possible.

In the quenching process, the austenite phase in the workpiece may be transformed into several different phases dependent on slope of the cooling curve, which is determined based on speed of quench, geometry of the workpiece being quenched, and material composition of the steel. Generally, three micro-structural constituents can be transformed from the austenite phase. They are martensite resulting from fast cooling, and pearlite and bainite from slower cooling.

The goal of hardening analysis is to find the martensite content to determine the hardness distribution in the workpiece. The kinetics of the austenite-martensite transformation during continuous cooling are generally expressed with Koistinen-Marburger law:[4]

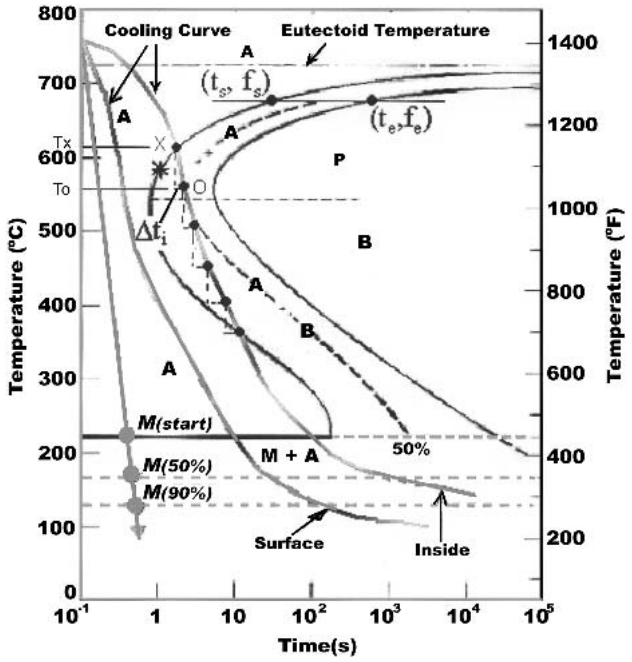

Fig. 2 Schematic of phase transformation kinetics in TTT diagram

$$f_m = (1 - \sum_j f_j)(1 - e^{-r(M_s - T)}) \quad \text{(Eq 15)}$$

where f_m is the fraction of martensite formed at temperature T; M_s is the martensite starting temperature of the metal, which is dependent upon carbon content in the material; r is a constant related to the composition of material; and f_j is the phases other than martensite formed in the quenching process, such as pearlite or bainite. They can be obtained based on Avrami type of equation

$$f(t) = 1 - e^{-k(T)t^{n(T)}} \quad \text{(Eq 16)}$$

where $f(t)$ is the fraction of pearlite or bainite after transformation time t under a specific temperature T in an isothermal transformation process; and $k(T)$ and $n(T)$ are the coefficients depending on time and volume fraction of isothermal transformation start point and end point in TTT diagram (Fig. 1), and $k(T)$, $n(T)$ can be expressed as:

$$n(T) = \frac{\ln\left[\frac{\ln(1 - f_s)}{\ln(1 - f_e)}\right]}{\ln\left(\frac{t_s}{t_e}\right)} \quad \text{(Eq 17)}$$

$$k(T) = \frac{-\ln(1 - f_s)}{t_s^{n(T)}} \quad \text{(Eq 18)}$$

where the subscription s, e note the starting and ending points of the isothermal transformation in TTT diagram.

Based on Eq 16, the fraction of pearlite or bainite formed

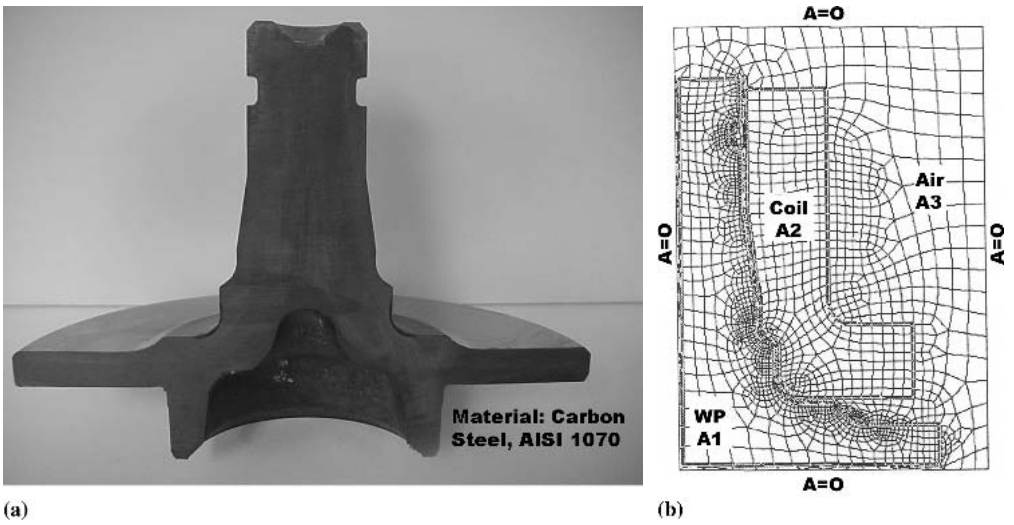

Fig. 3 FEA model and mesh of an automotive spindle: **(a)** automotive spindle; **(b)** FEA model

during quenching process can be determined by the following two methods.

Method 1: The continuous cooling curve can be discretized into a series of infinitesimal isothermal transformation processes; in each infinitesimal time period Δt_i, formed fraction of pearlite or bainite can be expressed by differentiating Eq 16 as:

$$\Delta f_i = (knt^{n-1}e^{-kt^n})\Delta t_i \quad \text{(Eq 19)}$$

where *n, k* are determined from Eq 17 and 18, and are all dependent on the temperature at which the isothermal transformation occurred in time step Δt_i. The total fraction of pearlite or bainite will be the summation of Δf_i:

$$f = \sum_i \Delta f_i \quad \text{(Eq 20)}$$

Method 2: It is also based on isothermal transformation process. As shown in Fig. 2,

(1) for one discrete transformation from point X to point O in time period Δt_i, the amount of transformation equals that on the isothermal diagram at mean temperature $\frac{1}{2}(T_x + T_o)$ for the same period started from the point with a star.
(2) with Eq 19 and 20, the amount of pearlite or bainite can be determined.

Once f_m is determined, it can be related to hardness HRC by a recursively built relationship based on test results of Ref. 7:

$$HRC = a(f_m)^2 + b(f_m) + c \quad \text{(Eq 21)}$$

Where constant *a, b, c* are only dependent on carbon content in the materials. For example, based on our calculation, $a = 77.84$, $b = -90.85$, $c = 75.28$ for AISI 1053; $a = 80.91$, $b = -97$, $c = 81.61$ for AISI 1070.

3. Finite Element Analysis

Due to the temperature-dependent nonlinear properties in induction heating process, analytical solutions are difficult to obtain. When surfaces with complex geometric shape are heat-treated, the problems become more cumbersome. In past years, several numerical approaches have been used for simulating induction-heating problems. But, finite element methods (FEM) appear to be superior to others such as finite difference methods.[8,9] Furthermore, general-purpose commercial finite element programs have been widely used in industry and are becoming more popular for engineering analysis and equipment design. These programs usually have a high capability for handling various geometries and specialized elements for a wide variety of applications including field problems, structures, and coupled problems. These capabilities can bring powerful tools to the analysis of induction heating system. In this work, a powerful FEA package, ANSYS57, was applied for modeling of induction hardening on an automotive spindle made from AISI 1070 carbon steel (Fig. 3).

Figure 3(a) shows the workpiece geometry. Due to axisymmetry, the system can be simplified as a two-dimensional problem. Figure 3(b) shows the geometry model of the spindle and the quadrilateral grids generated in ANASYS package. The geometry of the workpiece represents the major characteristics of spindle hardening surface, an induction coil is designed according to spindle surface with a uniform air gap. A rectangular computational domain is taken to enclose the workpiece and coil, and on its boundaries, the magnetic vector potential A is set as zero as the boundary conditions, following previous work by Roplekar.[7] For the convenience of dealing with different components of the domain, areas A1, A2, and A3 are set for workpiece, coil, and air region, respectively. Initial condition is set as $T = 25$ °C for all three areas.

Due to the strong variation of materials properties with temperature, induction heating is a highly non-linear system. Hence, it has to be solved in a coupled manner, in which the material electromagnetic and thermal properties are updated at

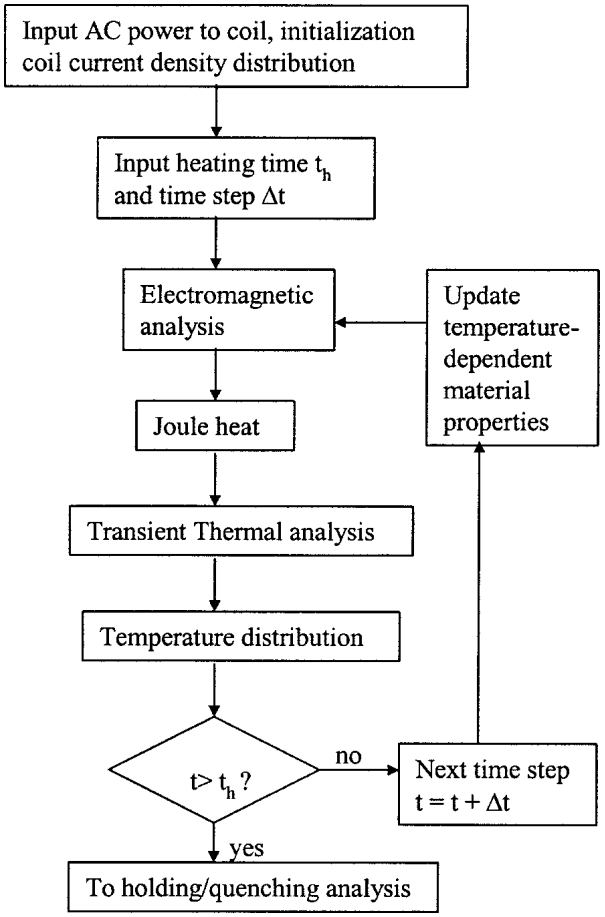

Fig. 4 Flow chart for coupled heating process

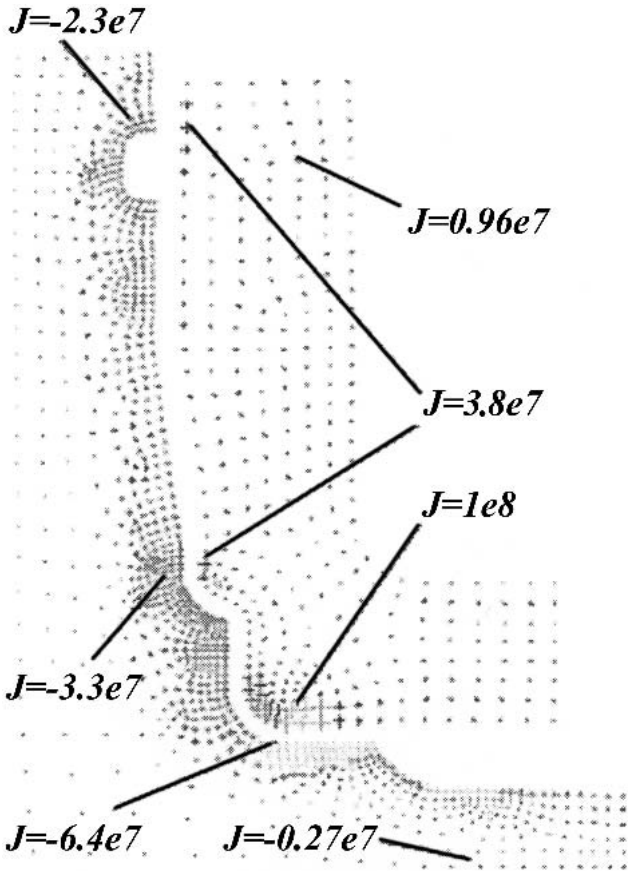

Fig. 5 Current density distribution

a new temperature in each loop until heating time is reached. The iteration loop is generally controlled by total heating time and time step determined in the codes. Simulation of the coupling procedure between the magnetic and thermal analysis is shown in Fig. 4.

4. Results and Discussion

At the beginning of the simulation, the initialization of current density distribution on each coil grid is a cumbersome but important step for desired temperature pattern control. Generally, the current density should be stronger (weak) in the part of the coil area neighboring concave (convex) in the workpiece. The arrangement of current density distribution for a specially desired heating pattern and hardening pattern may guide real inductor design, in which strong current density distribution induced by strong magnetic field can be fulfilled through use of magnetic concentrator.[10] The heating time, t_h, and time resolution, Δt, are generally controlled by the desired heating pattern and computational convergence issues. The determination of t_h is also an important consideration for induction system design.

The average input AC current density to each element of the coil is $J = 1.26e^7$ (A/m^2), frequency is $f = 9600$ Hz. Due to the complexity of the hardening surface, higher current density values are set at three regions of the coil where concaves of the workpiece are neighbors. The heating time and time step were set as $t_h = 7.05$ s, $\Delta t = 0.05$ s, respectively, based on practical industrial hardening process.

Figure 5 shows the current density distribution in the induction coil and the induced eddy current density distribution in the workpiece. Corresponding to bigger current density area of coil, the induced current density in the workpiece is also much larger under the surface of a concave region. Due to the skin effect, a large value of current density is distributed in a thin layer under the heat-treating surface. In other parts of the workpiece, the eddy current density decreases with the distance increase away from the workpiece surface.

Figure 6 shows the temperature distribution in the workpiece during induction heating at two times: $t = 2$ s and 7.05 s. The austenitized layer ($T > 815$ °C) under the workpiece surface gradually becomes thicker with heating time; this shows the propagation of heat conduction effect in the workpiece. Generally, locations such as convex are easily overheated due to heat transfer and concentration effects. After the first 2 s of heating, location of maximum temperature is formed at the most sharp convex. In our case, three convex regions have high temperature values. The total heating time is determined such that sufficient austenization area is formed.

Figure 7 shows heating curves of some interesting locations marked in Fig. 6(b). C1, C2, . . . C6 represents points along a

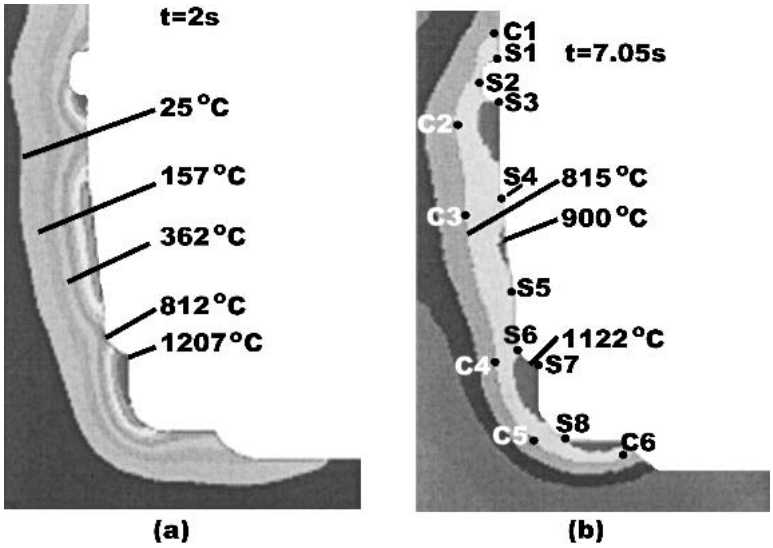

Fig. 6 Temperature field evaluation in induction heating process. $F = 9600$ Hz, $s = 1.27$ mm, $J = 1e^7$ (A/m^2). **(a)** $t = 2$ s; **(b)** $t = 7.05$ s

temperature contour line ($T = 815$ °C), which is the inner bound of austenitized zone (815 °C-1380 °C for AISI 1070 carbon steel). S1, S2, . . . S8 means surface points. Heating curves in Fig. 7(a) show different heating routes of the interest inside locations, though their initial and final temperature are almost the same. Inside locations are mainly heated through the heat conduction effect with heat flux from the skin effected by a thin layer under the surface. The shape of heating curves are determined, in large extent, by their geometric location in the workpiece. The heating curves in Fig. 7(b) show the temperature curves at surface locations. After the first sharp heating stage, heat transfer effect begins to balance the electromagnetic induced Joule heat, and heating curves gradually trend to more stable temperature values.

A severe water quenching process is used in this case with high-pressure water jets at a speed of 2 m/s, a flow rate of 3.78 L/s, and a minimum pressure at 60 psi. Based on these parameters and analysis of the quenching process, a forced convection model is used in the simulation. The quenching time is 40 s.

Figure 8 shows the evolution of the temperature field in the workpiece in quench process. High temperature region varies with time, and moves away from heat treated surface to the area (lowest temperature region before quenching) with maximum potential to absorb heat. The cooling rate is much higher at first stage. For example, the maximum temperature before the quenching is about 1033 °C; after 0.5 s, it decreases to 906 °C (Fig. 8a). This results in a cooling rate of 254 °C/s. From $t = 0.5$-2 s, cooling rate decreases to 77 °C/s.

Figure 9 shows the cooling curves of some interest locations in the workpiece. Due to the forced convection and radiation effect, the sharp cooling curves of surface points (such as C1) keep them from intersecting with the TTT diagram of material. For AISI 1070 carbon steel, the nose of TTT curves is at 2 s and 540 °C. The cooling curves for those inside locations (C2-C5) are mild because only heat conduction, driven from surface convection and radiation, plays a cooling role. Most of cooling curves of these inside points will intersect with the TTT dia-

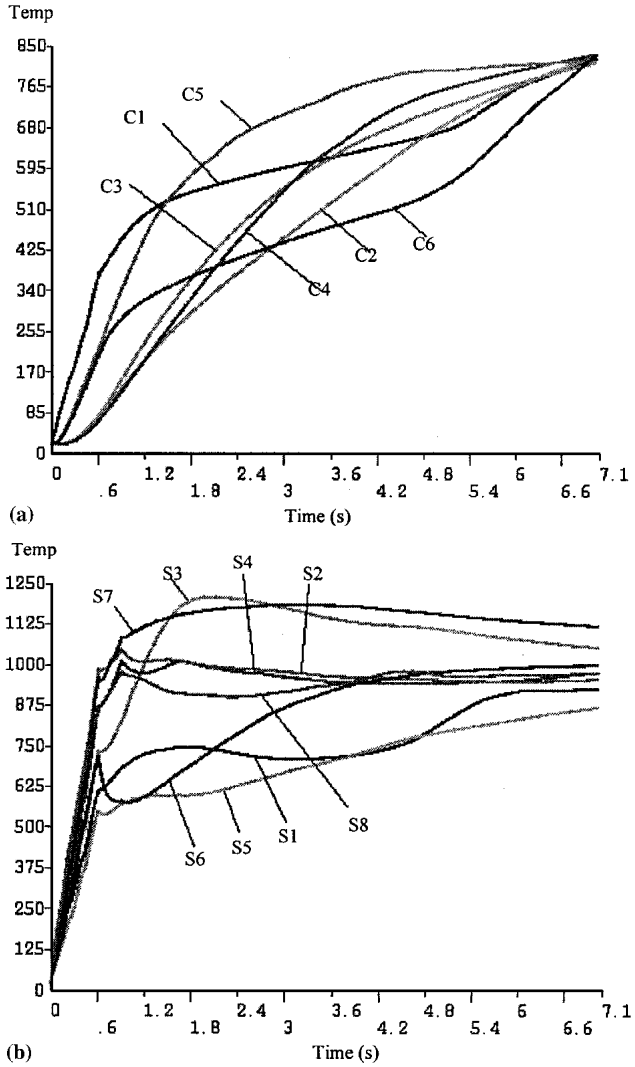

Fig. 7 Heating curves of interesting locations: **(a)** inside points along austenitized zone; **(b)** surface points

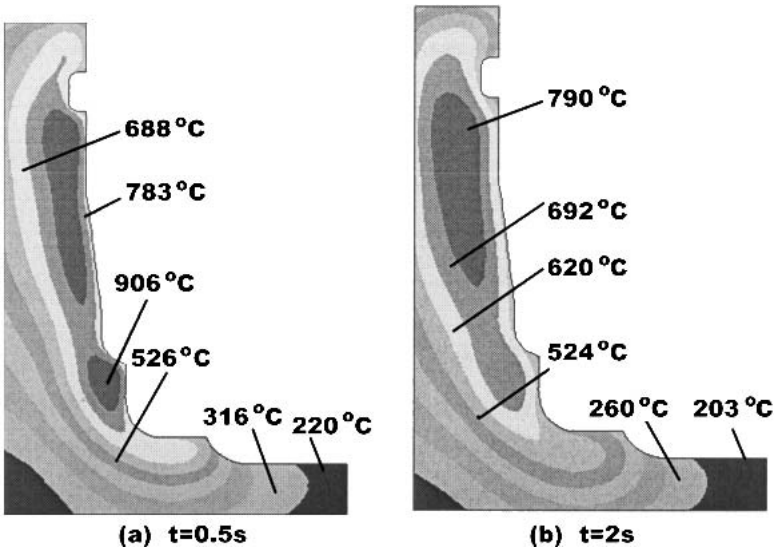

Fig. 8 Temperature field evaluation in quenching process: **(a)** $t = 0.5$ s; **(b)** $t = 40$ s

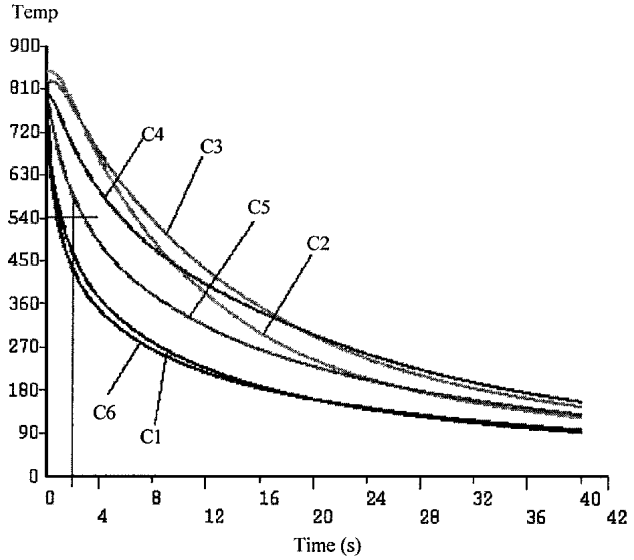

Fig. 9 Cooling curves of selected locations

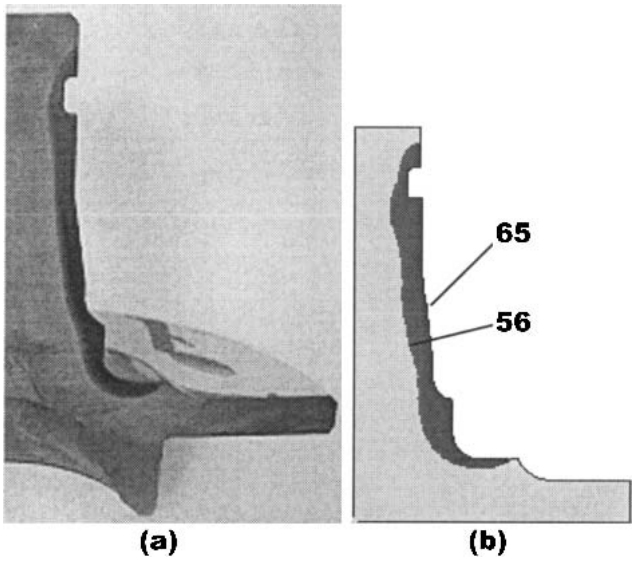

Fig. 10 Comparison of hardening pattern: **(a)** practical result; **(b)** modeling result

gram and will result in the austenite-pearlite and austenite-bainite transformation. The fraction of martensite formed for these locations will be determined with Eq 15-20. The detailed algorithm will be described in another paper.

Hardness is calculated using Eq 21 upon martensite content is determined based on Eq 15. Figure 10 shows the comparison of hardness pattern from the numerical simulation and practical results. It shows a good match. In Fig. 10(b), bounds of hardened zone are regulated based on hardness value in the range of *HRC* = 56-65. Mean case depth (δ) of hardened zone will be used to study the effects from input average AC current density (*J*), AC frequency (*f*), and gap (*s*) between the coil and workpiece.

Figure 11 shows trends of case depth δ variation with *J*, *f*, and *s*. Figure 11(a) shows case depth increases with power density (*J*), because larger power density (*J*) can result in stronger magnetic field intensity and induce larger eddy current and Joule heat in the workpiece. Figure 11(b) shows case depth decreases with input AC frequency (*f*) due to skin depth effects. Figure 11(c) shows case depth slightly decreases with air gap (*s*) because induced heat diminished in the workpiece.

5. Conclusion

A numerical modeling and simulation system is developed based on a commercial FEA package, ANSYS. The system can simulate the entire hardening processes from electromagnetic-induced heating and quench cooling, to final hardening. The comparison of hardening pattern between practical case and

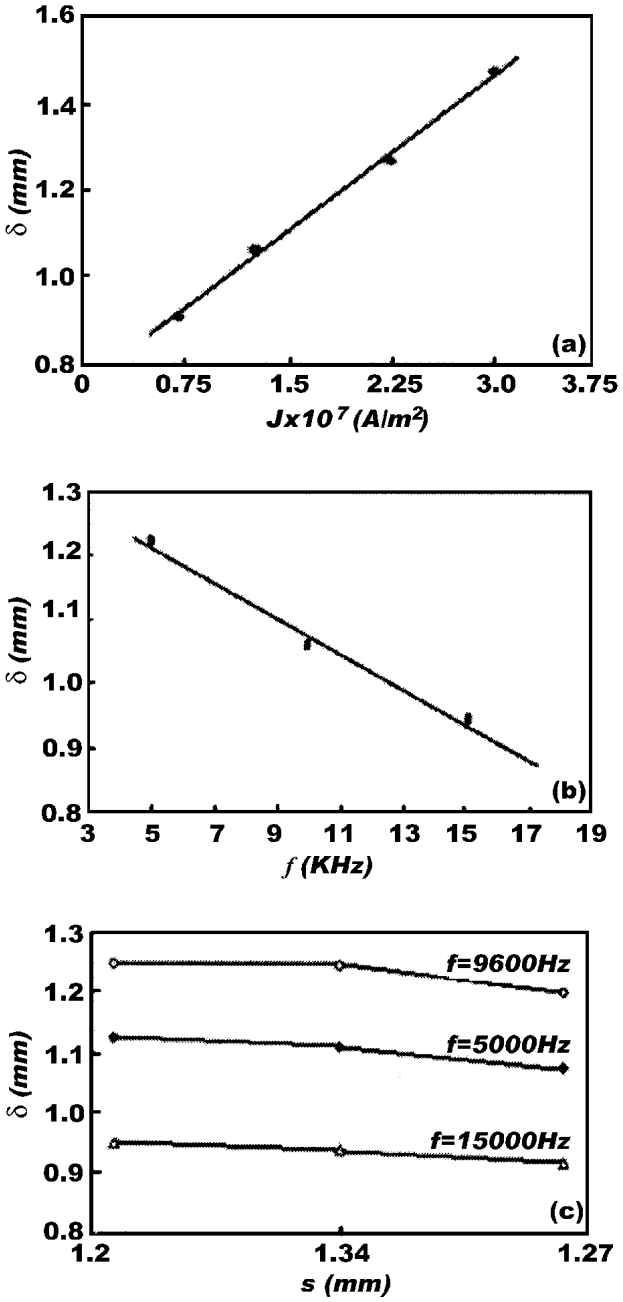

Fig. 11 Case depth variation with *J, f,* and *s*

modeling results shows a good match and indicates that the developed modeling system may be a powerful tool for induction system design.

This modeling and simulation system provides a means to determine key parameters in the induction hardening system design, especially in phase transformation area and hardness determination. Detailed schemes are described and a relationship between martensite content and hardness was established based on a historic database with mathematic curve fitting techniques.

The capabilities of this modeling and simulation system include predicting the transient temperature distribution and heating or cooling curves, estimating the volume fraction of different metal phases formed in the quenching process based on phase transformation kinetics, and providing a desired heating and hardening pattern based on the design of coil current density distribution which suggests the use of magnetic concentrator in practical situations for induction coil design.

Acknowledgments

The authors thank Dr. Q. Lu for the framework built for the first stage of the project. Thanks also to Dr. D.W. Yen, Mr. C. Price, and Mr. A. Mandeville, in Delphi, and W. Stuehr and D. Lynch from Induction Tooling, for providing important materials and information. Finally, partial financial support from the Center for Heat Treating Excellence (CHTE) at WPI is highly appreciated.

References

1. M.V.K. Chair: "Finite Element Solution of the Eddy-Current Problem in Magnetic Structures," *IEEE Trans. PAS,* 1973, *93*(1), p. 62.
2. V.S. Nemkov and R. Goldstein: "Computer Simulation for Design of Induction Heat Treating Processes and Work Coils" in *19th ASM Heat Treatment Society Conf. Proc. Including Steel Heat Treating in the New Millennium,* 1999, pp. 154-61.
3. R. Pakalapati, L. Jin, T.N. Farris, and S. Chandrasekar: "Simulation of Quenching of Steels: Effects of Different Multiphase Constitutive Models" in *19th ASM Heat Treatment Society Conf. Proc. Including Steel Heat Treating in the New Millennium*, 1999, pp. 416-23.
4. D. Koistinen and R. Marburger: "A General Equation Prescribing the Extent of the Austenite-Martensite Transformation in Pure Iron-Carbon Alloys and Carbon Steels," *Acta Metall.,* 1959, *7*, p. 59.
5. M. Avrami: "Kinetics of Phase Change," I, *J. Chem. Phys.,* 7, 1103 (1939).
6. J.P. Sturgess and T.W. Presion: "An Economic Solution for 3D Coupled Electromagnetic and Thermal Eddy Current Problems," *IEEE Trans., Magn.,* 1992, *27*(2), pp. 1267-69.
7. K. Thelning: *Steel and Its Heat Treatment,* 2nd ed., Butterworths, 1984.
8. M. Enokizono, T. Todaka, and S. Nishimura: "Finite Element Analysis of High Frequency Induction Heating Problems Considering Inhomogeneous Flow of Exciting Currents," *IEEE Trans., Magn.,* 1999, *35*(3), pp. 1646-50.
9. H.H.J.M. Janssen, E.J. W. ter Maten, and van Houwelingen: "Simulation of Coupled Electromagnetic and Heat Dissipation Problems," *COMPUMAG-Miami*, 1993, pp. 42-43.
10. T.J. Learman: "Formable and Thermal Hardenable Concentrator Enhances Induction Heating Process," *Ind. Heat.,* 1995, *62*(6), pp. 39-42.